EJECTA PATTERN OF OBLIQUE IMPACTS ON THE MOON FROM NUMERICAL SIMULATION.
X.-Z. Luo[1], M.-H. Zhu[1], and M. Ding[1], [1]State Key Laboratory of Lunar and Planetary Sciences, Macau University of Science and Technology, Macau, China (mhzhu@must.edu.mo).

Introduction: Nearly all asteroids impact a planet at oblique incident angles. Impact probability on a planet indicates that the most probable angle of impact is 45° from the surface plane, and ~ 50% of all impacts occur between 30° to 60° [1, 2]. Laboratory experiments of oblique impacts show that the ejecta pattern varies significantly with incident angles [3, 4]. For example, the ejecta blanket changes from symmetric to asymmetric shape with more ejecta depositing in the downrange as the impact angle decreases. At certain impact angle, a V-shaped zone of avoidance (ZoA) emerges in the uprange due to the absence of ejecta deposits. For extremely low angle "grazing" cases, impacts even lead to a lack of ejecta in both the downrange and the uprange, forming a "butterfly" ejecta pattern.

Similar ejecta patterns between tens-to-hundreds kilometer-scale craters (or basins) on the Moon and centimeter-scale craters in laboratory experiments have been observed [5]. As a consequence, the results of laboratory experiments have been extrapolated to infer the corresponding impact angles from remote-sensing observations for impact craters (or basins) on the Moon. However, the ejecta patterns of large-scale craters (or basins) and laboratory craters with similar impact angles may be different owing to their difference in scales. It was suggested that the asymmetry level of the ejecta pattern is controlled by cratering efficiency, which is related to impact angles [6-8] and the scaling parameter $\pi_2 = 1.61gd/U^2$ for gravity-dominated craters [9], where g is the gravity of target, and d, U are diameter and velocity of the impactor. In the gravity-dominated crater-forming regime, the size of asteroids hitting the Moon varies from several hundred meters to tens of kilometers, and the impact velocity varies from about 10 to 30 km/s [e.g., 10]. Therefore, kilometer-scale crater-forming impacts on the Moon have much larger π_2 than those from laboratory experiments, which may produce different ejecta patterns from the laboratory experiments for impacts with similar angles. Here, we use three-dimensional shock physics simulation to bridge the gap between laboratory experiments and large-scale natural impacts occurred on the Moon, and focus on the combined effect of impact angles and impactor diameters on the ejecta patterns.

Numerical Modeling: We use the iSALE-3D shock physics code [7] to simulate the cratering process of oblique impacts. We vary the impactor diameter (from 1 km to 120 km) and angles (20°, 30°, 45°, and 60°) for a typical impact velocity of 15 km/s, assuming the impactor and target materials are both dunite in our simulations. For each model, we simulate the entire excavation stage and track the launch velocities and positions when materials move above the pre-impact surface. We then calculate the ejecta deposition on a flat surface assuming parabolic trajectories. The ejecta thickness at any evenly spaced grid point over the deposition surface is calculated by dividing the total volume of tracers landing on each grid by the grid area. We consider the effect of the ejecta flow on the final deposition pattern is limited without significant sliding after ejecta hit the surface, and we do not take into account the effects of secondary cratering and local topographies.

Results and Discussion: Our modeled ejecta patterns for 6- and 60-km-diameter impactors are shown, for comparison, in Figs. 1 and 2. A contour level at ejecta thickness equal to 0.001 impactor radius is representative of the ejecta blanket (ejecta pattern) outline in our simulations. For the 6-km impactor (Fig. 1), the ejecta patterns with relatively low impact angles of 20° and 30° are characterized by a notable V-shaped ZoA lacking ejecta deposits in the uprange. No uprange ZoA can be found at greater impact angles of 45° and 60°, although the ejecta patterns are still asymmetric, with the entire ejecta blanket offset towards the downrange.

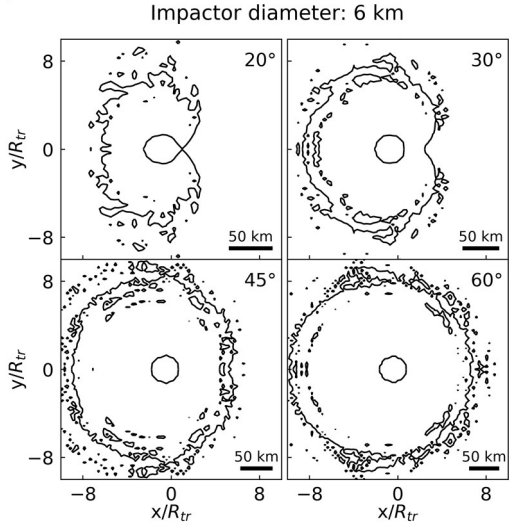

Figure 1. Ejecta patterns of oblique impacts at varied impact angles produced by a 6-km-diameter impactor. The impact direction is from right to left. Distances from the impact center are normalized by the transient crater radius, R_{tr}.

For the 60-km-diameter impactor (Fig. 2), an uprange ZoA can be recognized at all four impact angles. Especially, an ejecta pattern of "butterfly" shape can be clearly seen at an impact angle of 20°, strikingly different from the 6-km-diameter impact case. Our results show that a larger π_2 (due to larger impactor) produces uprange ZoA at higher impact angles.

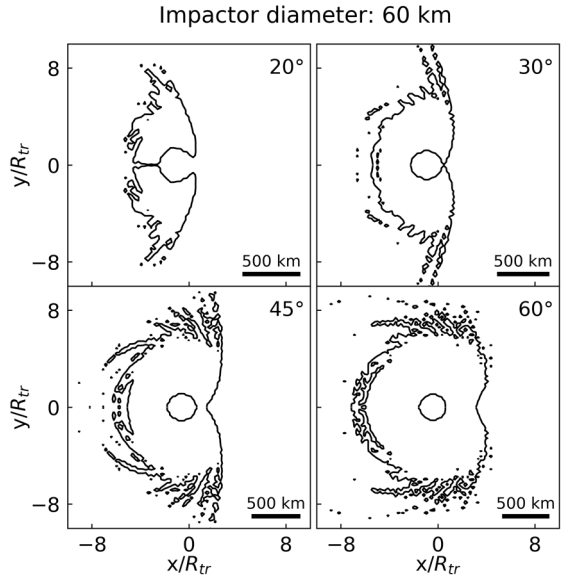

Figure 2. Similar to Fig. 1 but for a 60-km-diameter impactor.

We then define a single metric ΔZoA, which is the distance between the vertex of uprange ZoA and the crater center (Fig. 3a), to quantify the asymmetry level of the ejecta pattern. A smaller ΔZoA is associated with a more "butterfly"-like ejecta pattern (see the ejecta patterns in Fig. 1 and Fig. 2), while a larger ΔZoA indicates more symmetric patterns.

Using this ΔZoA, we further quantify the effects of impactor sizes and impact angles. Fig 3a clearly shows that the normalized ΔZoA decreases with increasing impactor-to-crater-diameter ratio d/D_{tr}, where d and D_{tr} are diameters of the impactor and the transient crater. This normalization is helpful to reduce data scattering, as data points in Fig. 3a now roughly lie on the same curve for all simulations. Fig. 3b shows the value of ΔZoA decreases with impact angles for the same impactor diameter. Note that for the 1-km- and 6-km-diameter impactors, no uprange ZoA is recognizable (within 10 times crater radii) at impact angles larger than 20° and 45°, respectively. The ZoA vertex could be closer to the crater rim for real craters on planets due to enlargement of crater diameter under gravitational collapse [e.g., 11].

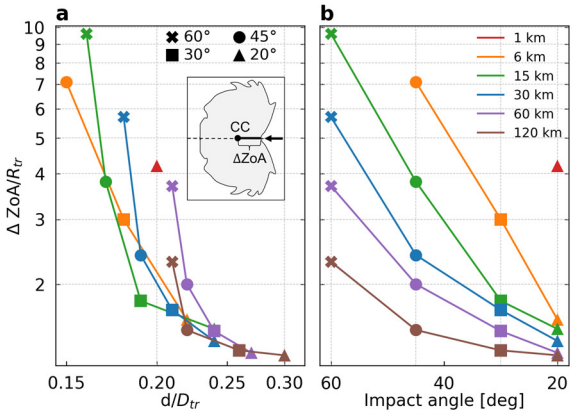

Figure 3. The normalized ΔZoA as a function of (a) impactor-to-crater-diameter ratio and (b) impact angle. The schematic diagram in (a) demonstrates our definition of ΔZoA. The arrow indicates impact direction.

We also ran a suite of simulations (results not shown here) at impact velocities of 10–30 km/s. The effects of impact velocity on the ejecta pattern, especially for larger craters, are limited comparing with the impactor size and angle. We note that as ejecta patterns also depend on gravity, the ejecta pattern is expected to be different for similar impacts on planets with different gravitational acceleration.

Conclusions: We numerically simulate the formation process of tens-to-hundreds kilometer-scale craters on the Moon and investigate their ejecta patterns as a function of impactor diameter and impact angle. Our results show that larger impactors produce more asymmetric ejecta patterns at the same impact angle, as predicted by [9]. Therefore, the prediction of impact angle for kilometer-scale craters on the Moon cannot be precisely derived from the comparative ejecta pattern in small-scale laboratory experiments.

Acknowledgements: This work is supported by the Science and Technology Development Fund, Macau (0079/2018/A2; 0020/2021/A1). We gratefully acknowledge the developers of iSALE-3D.

References: [1] Gilbert G. (1893) *Bull. Philos. Soc. Wash., XII,* 241-292. [2] Shoemaker E.M. (1962) *Physics and Astronomy of the Moon*, 283-359. [3] Gault D.E. & Wedekind J.A. (1978) *Proc. LPSC, 9,* 3843-3875. [4] Hessen K. et al. (2007) *LPSC, 1338*, 2141. [5] Herrick R.R. and Forsberg-Taylor N.K. (2003) *Meteoritics & Planet. Sci., 38(11),* 1551-1578. [6] Chapman C. R. & McKinnon W. B. (1986) *Satellites*, 492-580. [7] Elbeshausen D. et al. (2009) *Icarus, 204(2),* 716-731. [8] Davison T. M. et al. (2011) *Meteoritics & Planet. Sci., 46(10)*, 1510-1524. [9] Shuvalov V. (2011) *Meteoritics & Planet. Sci., 46(11),* 1713-1718. [10] Minton D.A. et al. (2015) *Icarus, 247,* 172-190. [11] Croft S.K. (1985) *JGR, 90(S02),* C828-C842.